

Exploring Intrinsic Magnetic Topological Insulators: The Case of EuIn_2As_2

Hao Liu,¹ Qi-Yi Wu,¹ Chen Zhang,¹ Jie Pang,^{2,3} Bo Chen,¹ Jiao-Jiao Song,¹ Yu-Xia Duan,¹ Ya-Hua Yuan,¹ Hai-Yun Liu,⁴ Chuan-Cun Shu,¹ Yuan-Feng Xu,⁵ You-Guo Shi,^{2,3} and Jian-Qiao Meng^{1,*}

¹*School of Physics, Central South University, Changsha 410083, Hunan, China*

²*Beijing National Laboratory for Condensed Matter Physics,*

Institute of Physics, Chinese Academy of Sciences, Beijing 100190, China

³*School of Physical Sciences, University of Chinese Academy of Sciences, Beijing 100049, China*

⁴*Beijing Academy of Quantum Information Sciences, Beijing 100085, China*

⁵*Center for Correlated Matter and School of Physics, Zhejiang University, Hangzhou 310058, China*

(Dated: Wednesday 24th July, 2024)

In this study, ultrafast optical spectroscopy was employed to elucidate the intricate topological features of EuIn_2As_2 , a promising candidate for a magnetic topological-crystalline axion insulator. Our investigation, focusing on the real-time evolution of topological states, unveiled a well-supported narrow surface magnetic gap ($2\Delta_0 \simeq 8.2$ meV) emerging at the antiferromagnetic transition temperature ($T_N \approx 16$ K). Below T_N , two extremely low-energy collective modes, ω_1 and ω_2 , with frequencies of ~ 9.9 and 21.6 GHz at $T = 4$ K, respectively, were observed, exhibiting strong temperature dependence. ω_1 may correlate with an acoustic phonon, while ω_2 is associated with a magnon. The results suggest that EuIn_2As_2 has the potential to manifest a magnetic topological-crystalline axion insulator, presenting a small magnetic energy gap on the (001) surface. The findings further our understanding of the interplay between magnetism and topology in this material, showcasing its potential for applications in quantum information processing and spintronics.

Topological insulators, a revolutionary class of quantum materials, manifest topological surface states within an insulating bulk [1, 2]. These surface states, protected by time-reversal symmetry (TRS), exhibit linear dispersion near Dirac points, rendering them impervious to non-magnetic perturbations. The introduction of additional magnetic order, disrupting TRS, results in magnetic topological materials with unique band topology, promising distinct quantum phenomena [3, 4]. Recent theoretical predictions highlight EuIn_2As_2 as a compelling candidate [5], boasting intrinsic magnetic order and a three-dimensional hexagonal structure.

EuIn_2As_2 possesses a layered centrosymmetric crystal structure (space group $P6_3/mmc$, No. 194) with alternating stacking of Eu^{2+} and $[\text{In}_2\text{As}_2]^{2-}$ layers along the c axis, undergoing a paramagnetic (PM) to antiferromagnetic (AFM) transition at the Néel temperature $T_N \approx 16$ K [6, 7]. Theoretical frameworks propose EuIn_2As_2 as a potential topologically nontrivial magnetic insulator, capable of hosting AFM axion insulator phases [5, 8–10]. Advances in theoretical calculations underscore the critical influence of magnetic moment orientation on emergent topological states, predicting a topological crystalline insulator phase with some gapless surface states emerging on (100), (010), and (001) surfaces for in-plane oriented magnetic moments [5, 10, 11] and a higher-order topological insulator phase with gapped surface states emerging on (100) and (001) surfaces for out-of-plane oriented magnetic moments [5]. Unlike previously discovered material systems, DFT calculations reveal that topological surface states in the stoichiometric form of EuIn_2As_2 are precisely located at the Fermi energy (E_F).

Despite progress in understanding, controversies persist, particularly regarding the nature of the axion-insulator phase. The existence of an energy gap in the surface state associated with TRS breaking remains under scrutiny. Previous mag-

netic measurements indicate A -type AFM order in EuIn_2As_2 [6, 7], but recent neutron diffraction [8] and resonant elastic x-ray scattering [9] experiments suggest a low-symmetry helical AFM order, also satisfying the symmetry requirements for an axion insulator.

Magnetotransport measurements reveal negative magnetoresistance, indicating robust spin scattering by localized magnetic moments [6, 12]. Scanning tunneling microscopy and spectroscopy (STM/STS) data show a partial surface state gap (~ 40 meV) below T_N , diminishing with increasing temperatures but remains finite above T_N [13]. ARPES confirms hole-type Fermi pockets [10–12], a heavily hole-doped surface state, and an inverted bulk bands in the AFM state [11], suggesting topological surface states are located above E_F . Notably, ARPES confirms surface states dominance near E_F , but fails to detect magnetic exchange gaps within them [10–12]. No ultrafast optical spectroscopy studies have yet probed the existence of a potential narrow energy gap near E_F .

Ultrafast optical spectroscopy serves as a powerful tool for probing the intricate low-energy electron dynamics in correlated materials [14], offering insights into the complex behaviors of systems such as transition metal dichalcogenides [15, 16], high-temperature superconductors [17–21], and heavy fermions [22–25]. Sensitivity to changes in the low-energy electronic structure, especially the opening of narrow energy gaps near the E_F that may lead to bottleneck effects [17–26], renders it particularly valuable. Additionally, ultrafast optical spectroscopy excels in detecting collective bosonic excitations, providing a reliable indicator for phase transitions [22–24]. While ultrafast optical spectroscopy probes a material's bulk to a certain depth, it can offer valuable insights into the dynamics of surface states under specific conditions, particularly when surface states dominate the electronic structure near E_F , such as topological insulators [27, 28].

Our study utilizes ultrafast optical spectroscopy to investigate the intricate topological states of EuIn_2As_2 , aiming to address current controversies and provide dynamic insights. Employing ultrafast techniques, we seek to unveil the real-time evolution of topological features, offering a nuanced understanding of the interplay between magnetism and topology in this fascinating material. The temperature-dependent quasiparticle relaxation reveals the onset of a likely narrow surface magnetic gap ($2\Delta_0 \simeq 8.2$ meV) at T_N . Below T_N , our measurements show the emergence of two extremely low-energy collective modes, ω_1 and ω_2 , with frequencies of ~ 9.9 and 21.6 GHz at $T = 4$ K, respectively, both exhibiting strong temperature dependence. The temperature- and fluence-dependent measurements suggest that ω_1 may correspond to an acoustic phonon, while ω_2 is associated with a magnon. Our results indicate that stoichiometric EuIn_2As_2 holds the potential for realizing a magnetic topological-crystalline axion insulator, characterized by a small magnetic energy gap on the (001) surface.

High-quality single crystals of EuIn_2As_2 were grown utilizing the self-flux method [29], demonstrating a T_N of approximately 16 K (Refer to Fig. S1 in the Supplemental Materials for the magnetic measurements [30]). We performed ultrafast time-resolved differential reflectivity measurements ($\Delta R/R$) at a center wavelength of 800 nm (~ 1.55 eV) using a 1 MHz Yb-based femtosecond (fs) laser oscillator [17]. These measurements were carried out on a freshly cleaved (001) surface under a high vacuum of 10^{-6} mbar. The pump and probe beams were focused on the sample at nearly normal incidence, with spot diameters of approximately $85 \mu\text{m}$ for the pump beam and $40 \mu\text{m}$ for the probe beam. The pump and probe beams were s - and p -polarized, respectively.

Figure 1(a) presents differential reflectivity $\Delta R/R$ of EuIn_2As_2 at various temperatures (4 K - 50 K) at a pump fluence of $\sim 53 \mu\text{J}/\text{cm}^2$. Photoexcitation induces an immediate changes in $\Delta R/R$, followed by multiple recovery processes with different lifetimes, indicating diverse relaxation pathways. The curves exhibit a pronounced temperature dependence. Notably, the peak around 0.7 ps transforms into a valley with decreasing temperature. Below T_N , damped oscillations appear after a few picoseconds. These observations differ from Wu et al. [36] (minimal temperature dependence). The discrepancy likely stems from the different pump wavelengths (800 nm vs. 400 nm). Above T_N , optical conductivity suggests a transition from the valence to the conduction band at a wavenumber corresponding to 800 nm. Below T_N , the AFM transition splits the valence band [35]. Therefore, transient reflectivity using an 800 nm pump wavelength offers a more sensitive probe of the AFM transition in EuIn_2As_2 compared to the approach employed by Wu et al. [36].

Figure 1(b) presents a 2D map of $\Delta R/R$ (pump-probe delay vs. temperature). The initial relaxation (~ 0.3 ps) reveals pronounced variations in $\Delta R/R$ near T_N , with a clear positive-to-negative signal transition. This behavior confirms $\Delta R/R$ effectiveness in capturing electronic structure changes during the AFM transition. It aligns with expectations [22] and sup-

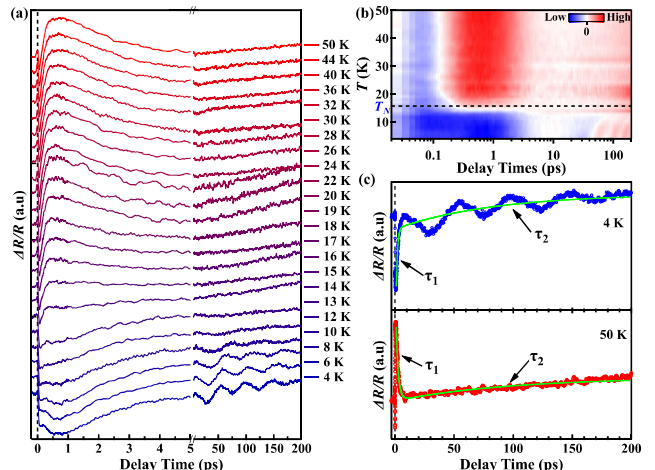


FIG. 1. (color online) (a) $\Delta R/R$ as a function of delay time over a temperature range from 4 to 50 K at pump fluence of $53 \mu\text{J}/\text{cm}^2$. Note the break in the x axis. (b) Two-dimensional pseudocolor map of $\Delta R/R$ as a function of temperature and delay time. (c) Illustration of fitting using Eq.(1) (upper panel: 4 K; bottom panel: 50 K). The arrows indicate the corresponding relaxation process.

ports prior findings from ARPES [10–12] and infrared spectroscopy [35] of significant alterations in the electronic structure during the AFM transition.

A quantitative analysis of quasiparticle dynamics was conducted to investigate its temperature-dependent behavior. We focus here on recombination processes occurring after electron-electron and electron-phonon thermalization, when carriers have already relaxed to the vicinity of the E_F [37]. The solid green lines in Fig. 1(c) suggests that the nonoscillatory response over a considerable time domain (~ 1 ps to 200 ps) fits well with a bi-exponential decay, using the expression

$$\frac{R(t)}{R} = \sum_{i=1,2} A_i \exp\left(-\frac{t-t_0}{\tau_i}\right) + C \quad (1)$$

where A_i is the amplitude and τ_i is the relaxation time of the i th nonoscillatory signal which describes carrier dynamics. C is a constant representing long-lifetime processes.

Figures 2(a) and 2(b) show the temperature dependence of extracted amplitude (A_1) and relaxation time (τ_1). Both exhibit anomalies near T_N , reflecting the influence of AFM order on electron-hole recombination [38]. A_1 displays a slow decrease followed by a rapid drop and sign reversal near T_N before saturating at lower temperatures. τ_1 shows a sharp rise (near divergence) at T_N . This behavior, similar to superconductors [17–21] and heavy fermion compounds [22–25], is attributed to a narrow energy gap (Δ) opening in the density of states (DOS) near E_F . The Rothwarf-Taylor (RT) model [26] successfully describes this behavior in correlated systems with a narrow energy gap near E_F [17–25]. Here, the RT model suggests that excited quasiparticles with energies greater than 2Δ decay by emitting high-frequency bosons that re-excite electron-hole pairs, creating a dynamic balance. Ac-

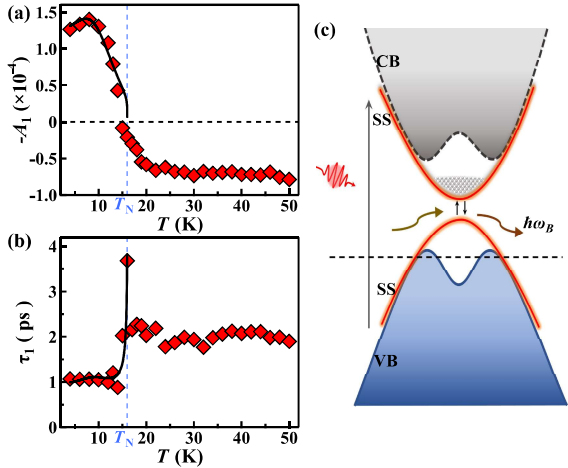


FIG. 2. (color online) (a) and (b) T -dependence of $-A_1$ and τ_1 , respectively. The black lines represent the RT model fitting curves. (c) A simplified cartoon schematic illustrating the relaxation process of photo-excited quasiparticles.

cording to the RT model, the T -dependent energy gap $\Delta(T)$ can be extracted from the following formulas [20–22]:

$$|A_1(T)| \propto \frac{\epsilon_l / [\Delta(T) + k_B T / 2]}{1 + \gamma \sqrt{2k_B T / \pi \Delta(T)} e^{-\Delta(T) / k_B T}} \quad (2)$$

$$\tau_1(T) \propto \frac{1}{[\delta(\beta n_T + 1)^{-1} + 2n_T](\Delta + \alpha T \Delta^4)} \quad (3)$$

$$n_T(T) = \frac{A(0)}{A(T)} - 1 \quad (4)$$

where ϵ_l is the absorbed laser energy density per unit cell, n_T is the density of quasiparticles thermally excited across the gap, and α , β , γ and δ are fitting parameters. Figure 2(a) presents a good fit to the absolute value of the amplitude $|A_1(T)|$ below T_N , as evidenced by the solid black lines, yielding an energy gap of $2\Delta_0 \simeq 8.2$ meV, with a typical Bardeen-Cooper-Schrieffer (BCS) form of the temperature dependence gap $\Delta(T) = \Delta_0[1 - (T/T_C)^{1/2}]$ [18, 22, 25]. We further calculated $n_T(T)$ using Eq. (4) and employed these values to fit the relaxation time $\tau_1(T)$ using Eq. (3) [Fig. 2(b)]. The good agreement between the fit and the data strongly supports our hypothesis of a narrow energy gap opening near E_F upon the development of the AFM order. The quasiparticle relaxation dynamics in EuIn_2As_2 is effectively described by the presence of a gap in the DOS near the E_F .

We note that STM/STS measurements [13] and DFT calculations [8, 10] indicate that the spin-orbit coupling induced bulk gap exhibits little variation across T_N and persists above T_N . This implies that the changes in A_1 and relaxation time τ_1 observed around T_N cannot be attributed to bulk band changes observed in prior ARPES studies [10, 11]. Previous theoretical calculations show that the AFM transition may lead to the opening of a gap at the Dirac cone of the surface state regardless of the out-of-plane AFM order [5, 10] or helical

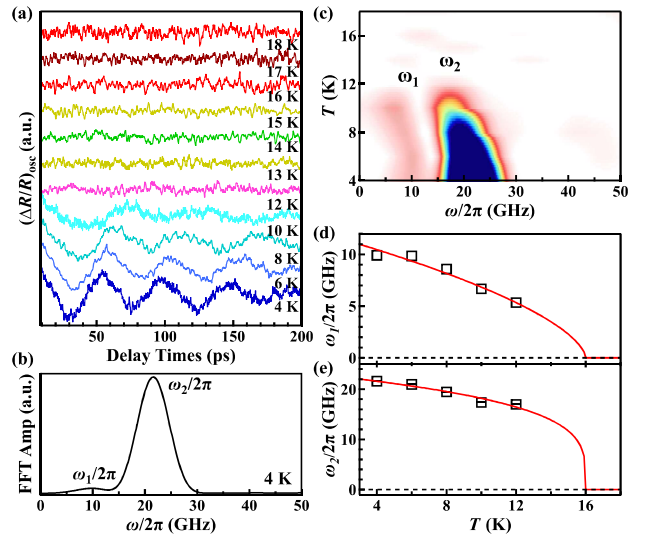


FIG. 3. (color online) (a) Extracted oscillations over a temperature range from 4 to 18 K at a pump fluence of $53 \mu\text{J}/\text{cm}^2$. Curves are shifted for clarity. (b) Fast Fourier transform (FFT) frequency-domain data at 4 K. (c) FFT spectrum color intensity map as a function of frequency and temperature. (d) and (e) The derived frequencies of ω_1 and ω_2 as a function of temperature. The red lines are fits described in the main text.

AFM order [8] at low temperatures. Intriguingly, this theoretical prediction aligns well with our experimental observations. Therefore, below T_N , we reasonably consider that the magnetic exchange interaction between the topological band and the localized Eu 4f spin results in the emergence of an energy gap in the surface state [Fig. 2(c)] [10–13]. The identification of a surface energy gap induced by AFM order in EuIn_2As_2 suggests the possibility that it may exhibit characteristics of an axion insulator [5, 8, 9].

It is noteworthy that the surface energy gap identified in our study differs from the findings of STM/STS [13] in two significant aspects. Firstly, the gap size we determined is considerably smaller than the one reported by STM/STS (~ 40 meV) [13]. Secondly, our observed gap manifests below the T_N , whereas the gap detected by STM/STS persists above T_N [13]. This gap difference can be attributed to the influence of specific surface terminations probed by STM/STS [13], as their technique is of atomic-scale resolution, while ultrafast optical spectroscopy integrates over a larger area. Time-resolved and angle-resolved photoemission spectroscopy (Tr-ARPES) will be essential for future work to precisely characterize the unoccupied band structure, particularly its temperature dependence and the gap position relative to E_F .

Following the low-fluence analysis, we investigated low-frequency collective bosonic excitations, known indicators of phase transitions [22, 23, 40]. Figure 3(a) depicts time-domain oscillations extracted from the low-temperature transient reflectivity data [Fig. 1(a)] after background removal. The oscillation periods and amplitudes vary with temperature, increasing and decreasing, respectively. Notably, the oscillation

tions are exclusively observed below T_N and vanish above it.

Oscillatory components were extracted by performing fast Fourier transform (FFT). Figure 3(b) presents two pronounced extremely low-energy modes, ω_1 and ω_2 , at frequencies of ~ 9.9 (i.e., 0.04 meV or 0.33 cm^{-1}) and ~ 21.6 GHz (i.e., 0.09 meV or 0.71 cm^{-1}) at a temperature of 4 K. Figure 3(c) displays the FFT spectrum as a function of frequency and temperature. The two Gigahertz modes, ω_1 and ω_2 , were exclusively observed at temperatures lower than T_N , with both frequencies consistently diminishing and experiencing softening as T_N is approached. The presence of the two extremely low-energy modes is limited to temperatures below T_N , suggesting they are either of magnetic origin or highly responsive to the magnetic ordering.

The extracted temperature dependence of ω_1 and ω_2 frequencies are plotted in Figs. 3(d) and 3(e), respectively. The temperature dependence of ω_1 and ω_2 can be effectively fitted using a mean-field-like T dependence [41]: $\omega = \omega(0)(1 - T/T_N)^{2\beta}$, where $T_N = 16$ K and β are the Néel temperature and critical exponent, respectively. This fitting yields zero-temperature frequencies of $\omega_1(0) \simeq 12.5$ GHz and $\omega_2(0) \simeq 23.2$ GHz, with corresponding β values of $\beta_{\omega_1} \simeq 0.31$ and $\beta_{\omega_2} \simeq 0.123$, respectively. $2\beta_{\omega_2}$ matches the expected value of 0.25 for a two-dimensional Ising system [42]. These results are consistent with the magnetic susceptibility measurements, suggesting that EuIn_2As_2 is a two-dimensional antiferromagnet [7, 12]. This noteworthy observation unequivocally confirms the intrinsically 2D character of EuIn_2As_2 's magnetic ordering, which has been observed in other antiferromagnets, such as two-dimensional antiferromagnet NiPS_3 [43]. At a pump fluence of $180 \mu\text{J}/\text{cm}^2$, Wu et al.'s time-resolved magneto-optical Kerr effect (TR-MOKE) measurements have revealed an 18 GHz spin precession mode under low magnetic fields, disappearing above T_N , while a persistent 35 GHz coherent acoustic phonon mode persists up to 25 K in high magnetic fields [36].

Considering that our measurements were conducted without the influence of a magnetic field, and given that the ω_2 mode disappears after a magnetic phase transition induced by intense pump fluence (to be discussed in detail later), we infer that the ω_2 mode originates from magnetic order, signifying its nature as a magnon. The localized Eu $4f$ spin, positioned approximately 1.7 eV below E_F and energetically separated from the initial optical excitation (1.55 eV), is effectively probed by ultrafast optical spectroscopy due to its strong interatomic exchange coupling with bulk topological bands. In EuIn_2As_2 , below T_N , electrons excited from In $5s$ and As $4p$ orbitals decay to the ground state via two primary mechanisms: electron-phonon coupling-induced spin flips and spin-orbit coupling-induced spin flips. Consequently, the localized Eu $4f$ spins undergo disorder through coupling with spin-flipped sp orbital electrons, leading to coherent magnon emission to conserve angular momentum. This process, akin to impulsive stimulated Raman scattering (ISRS) via spin-flip scattering, resembles an ultrafast inverse Cotton-Mouton effect, where the linearly polarized excitation

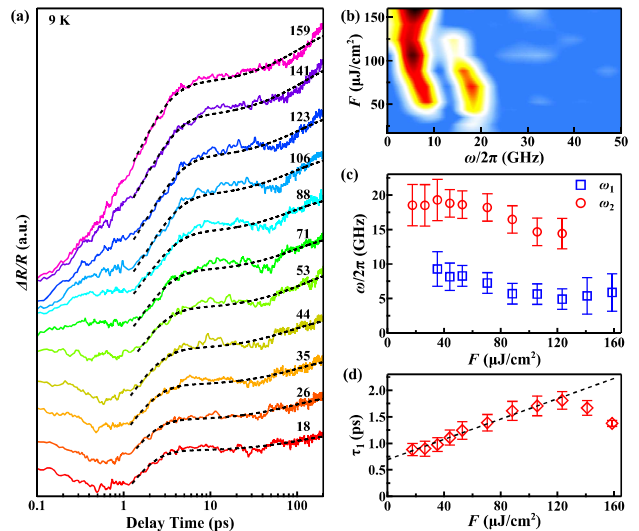


FIG. 4. (color online) (a) Fluence dependence of the $\Delta R/R$ as a function of delay time at 9 K over a long time scales. The black solid lines are Eq. (1) fits. (b) FFT spectrum color intensity map as a function of frequency and fluence. (c) The derived frequencies of ω_1 and ω_2 as a function of fluence. (d) Fluence dependence of τ_1 . The black dashed line represents the linear fit to the low fluence data.

pulse acts on spins as a short effective field pulse [43–45]. Ultrafast optical spectroscopy functions as a powerful tool for characterizing nonequilibrium spin dynamics and their intricate interplay with electrons and the lattice. The temperature evolution of the lower-frequency oscillation ω_1 differs, exhibiting distinct critical parameters compared to ω_2 . However, with the above dataset, we are unable to ascertain the origin of ω_1 .

In light of the complex magnetic structure revealed by low-temperature magnetization and magnetotransport measurements in EuIn_2As_2 [12], indicating the potential for an external field-induced phase transition, we conducted a fluence-dependent measurement at 9 K (Fig. 4(a)) to explore the characteristics of two modes and investigate potential photon-induced transient phase transitions. The $\Delta R/R$ response exhibits notable variations, with the well-defined reflectivity valley structure around 0.7 ps progressively suppressed and disappearing under high fluence (beyond $123 \mu\text{J}/\text{cm}^2$). The simplification of the reflectivity curve's lineshape implies the closure of specific relaxation channels as pump fluence surpasses the threshold [Refer to Fig. S2 in the Supplementary Materials [30]]. For a detailed analysis of oscillations and quasiparticle relaxation, we applied Eq. (1) to fit the fluence-dependent transient reflectivity beyond ~ 1 ps, achieving a good fit, as illustrated by the black dashed lines in Fig. 4(a).

FFT was utilized to extract the oscillations, and Fig. 4(b) presents the FFT spectrum in terms of frequency and fluence. Notably, ω_1 is challenging to discern at low fluence, while ω_2 becomes indiscernible at high fluence. The derived frequencies of ω_1 and ω_2 , displayed in Fig. 4(c), offer further insights. For fluences below $\sim 71 \mu\text{J}/\text{cm}^2$, ω_2 remains nearly

constant, subtly softening at higher fluence, and becoming undetectable beyond $123 \mu\text{J}/\text{cm}^2$. In contrast, ω_1 , initially indiscernible at low fluence, exhibits gradual softening and even slight abnormal hardening beyond $123 \mu\text{J}/\text{cm}^2$. In addition, Fig. 4(b) shows that the FFT amplitude of the ω_1 mode increases with the rise in pump fluence. The derived τ_1 was plotted in Fig. 4(d) as a function of pump fluence. Initially, τ_1 increases almost monotonically linearly with fluence, but beyond $123 \mu\text{J}/\text{cm}^2$, it decreases with further fluence, aligning partially with observations in MnBi_4Te_7 , where an increase in relaxation time with fluence was reported [38]. Calculations suggest that ω_1 couldn't be a coherent acoustic phonon induced by thermal stress (See details in the Supplementary Materials [30]). Therefore, we consider that the ω_1 mode might be excited by acoustic waves through a laser-induced magnetoelastic mechanism [46, 47]. However, further experiments and theoretical models are required to determine the origin of ω_1 .

To address the reduced τ_1 and the anomalous behavior of two modes beyond $123 \mu\text{J}/\text{cm}^2$, we considered two possibilities. Firstly, intense pumping causing pronounced heating, elevating the temperature of the illuminated area. Despite the lack of direct low-temperature thermal conductivity measurements [48], a preliminary estimation at 9 K was conducted for EuIn_2As_2 . The observed lower resistivity in EuIn_2As_2 [6, 7, 12] compared to its newly formed layered compound, $\beta\text{-EuIn}_2\text{As}_2$ [49], along with the higher specific heat in EuIn_2As_2 [7] than in $\beta\text{-EuIn}_2\text{As}_2$ [49], suggests that the thermal conductivity of EuIn_2As_2 possibly exceeds that of $\beta\text{-EuIn}_2\text{As}_2$ [49]. Consequently, at 9 K, the estimated thermal conductivity of EuIn_2As_2 is approximately 40 W/m-K. This estimation aligns with various measurements [6, 7, 10–12], including ARPES [10–12], supporting the characterization of EuIn_2As_2 as a metal. Considering optical constants [35] and a worst-case scenario (base temperature of 9 K and excitation density of $159 \mu\text{J}/\text{cm}^2$), a sample steady-state heat diffusion model [21] suggests that the average laser-induced heating in EuIn_2As_2 is less than 0.8 degrees and can be neglected. Secondly, a photo-induced rapid nonthermal phase transition, such as the quenching of magnetic order [21, 22, 50]. High fluence likely disrupts the AFM order and closes the surface states energy gaps created by antiferromagnetism, facilitating the rapid relaxation of excited carriers to the ground state. This interpretation aligns with the closure of specific relaxation channels, suggesting a photo-induced phase transition characterized by a prolonged transient magnetic phase transition.

In summary, ultrafast optical spectroscopy of EuIn_2As_2 reveals a key step towards its confirmation as a magnetic topological-crystalline axion insulator. A narrow, highly probable surface magnetic gap ($2\Delta_0 \simeq 8.2 \text{ meV}$) emerges precisely at the Néel temperature ($T_N \approx 16 \text{ K}$). Additionally, the identification of two low-energy collective modes - ω_1 (likely an acoustic phonon) and ω_2 (attributed to a magnon) - below T_N clarifies the intricate interplay between magnetism and topology. These findings resolve existing controversies

and highlight EuIn_2As_2 as a promising platform for exploring novel quantum phenomena at the magnetism-topology interface. The observed temperature and fluence dependence of ω_1 and ω_2 underscore the nature of EuIn_2As_2 . This work paves the way for future investigations into manipulating and exploiting magnetic topological-crystalline axion insulator phases.

This work was supported by National Key Research and Development Program of China (Grant No. 2022YFA1604204), the National Natural Science Foundation of China (Grant Nos. 12074436, U2032204, U22A6005, and 12374163), the Science and Technology Innovation Program of Hunan province (Grant No. 2022RC3068), the Strategic Priority Research Program of the Chinese Academy of Sciences (Grants No. XDB33010000), the Changsha Natural Science Foundation (Grant No. kq2208254), and the Fundamental Research Funds for the Central Universities of Central South University. We are grateful for resources from the High Performance Computing Center of Central South University.

* Corresponding author: jqmeng@csu.edu.cn

- [1] M. Z. Hasan and C. L. Kane, *Rev. Mod. Phys.* **82**, 3045 (2010).
- [2] X. L. Qi and S. C. Zhang, *Rev. Mod. Phys.* **83**, 1057 (2011).
- [3] B. A. Bernevig, C. Felser, and H. Beidenkopf, *Nature* **603**, 41 (2022).
- [4] Y. F. Xu, L. Elcoro, Z. Song, B. J. Wieder, M. G. Vergniory, N. Regnault, Y. Chen, C. Felser, and B. A. Bernevig, *Nature* **586**, 702 (2020).
- [5] Y. F. Xu, Z. Song, Z. Wang, H. Weng, and X. Dai, *Phys. Rev. Lett.* **122**, 256402 (2019).
- [6] A. M. Goforth, P. Klavins, J. C. Fettinger, and S. M. Kauzlarich, *Inorg. Chem.* **47**, 11048 (2008)
- [7] P. F. S. Rosa, C. Adriano, T. M. Garitezi, R. A. Ribeiro, Z. Fisk, and P. G. Pagliuso, *Phys. Rev. B* **86**, 094408 (2012).
- [8] S. X. M. Riberolles, T. V. Trevisan, B. Kuthanazhi, T. W. Heitmann, F. Ye, D. C. Johnston, S. L. Bud Ko, D. H. Ryan, P. C. Canfield, A. Kreyssig, A. Vishwanath, R. J. McQueeney, L. L. Wang, P. P. Orth, and B. G. Ueland, *Nat. Commun.* **12**, 999 (2021).
- [9] J. Soh, A. Bombardi, F. Mila, M. C. Rahn, D. Prabhakaran, S. Francoual, H. M. Rønnow, and A. T. Boothroyd, *Nat. Commun.* **14**, 3387 (2023).
- [10] S. Regmi, M. M. Hosen, B. Ghosh, B. Singh, G. Dhakal, C. Sims, B. Wang, F. Kabir, K. Dimitri, Y. Liu, A. Agarwal, H. Lin, D. Kaczorowski, A. Bansil, and M. Neupane, *Phys. Rev. B* **102**, 165153 (2020).
- [11] T. Sato, Z. Wang, D. Takane, S. Souma, C. Cui, Y. Li, K. Nakayama, T. Kawakami, Y. Kubota, C. Cacho, T.K. Kim, A. Arab, V.N. Strocov, Y. Yao, and T. Takahashi, *Phys. Rev. Res* **2**, 033342 (2020).
- [12] Y. Zhang, K. Deng, X. Zhang, M. Wang, Y. Wang, C. Liu, J. W. Mei, S. Kumar, E.F. Schwier, K. Shimada, C. Y. Chen, and B. Shen, *Phys. Rev. B* **101**, 205126 (2020).
- [13] M. Gong, D. Sar, J. Friedman, D. Kaczorowski, S. Abdel Razeq, W. C. Lee, and P. Aynajian, *Phys. Rev. B* **106**, 125156 (2022).
- [14] D. N. Basov, R. D. Averitt, D. van der Marel, M. Dressel, and

- K. Haule, *Rev. Mod. Phys.* **83**, 471 (2011).
- [15] S. X. Zhu, C. Zhang, Q. Y. Wu, X. F. Tang, H. Liu, Z. T. Liu, Y. Luo, J. J. Song, F. Y. Wu, Y. Z. Zhao, S. Y. Liu, T. Le, X. Lu, H. Ma, K. H. Liu, Y. H. Yuan, H. Huang, J. He, H. Y. Liu, Yu-Xia Duan, and J. Q. Meng, *Phys. Rev. B* **103**, 115108 (2021).
- [16] J. Qi, I. Miotkowski, H. Cao, Y. P. Chen, Y. Wu, S. Qiao, and Z. Jiang, *Appl. Phys. Lett.* **97**, 182102 (2010).
- [17] C. Zhang, Q. Y. Wu, W. S. Hong, H. Liu, S. X. Zhu, J. J. Song, Y. Z. Zhao, F. Y. Wu, Z. T. Liu, S. Y. Liu, Y. H. Yuan, H. Huang, J. He, S. L. Li, H. Y. Liu, Y. X. Duan, H. Q. Luo, and J. Q. Meng, *Sci. China-Phys. Mech. Astron.* **65**, 237411 (2022).
- [18] Q. Y. Wu, C. Zhang, Z. Z. Li, W. S. Hong, H. Liu, J. J. Song, Y. Z. Zhao, Y. H. Yuan, B. Chen, X. Q. Ye, S. L. Li, J. He, H. Y. Liu, Y. X. Duan, H. Q. Luo, and J. Q. Meng, *Phys. Rev. B* **108**, 205136 (2023).
- [19] Q. Y. Wu, J. Q. Meng, *Sci. Sin-Phys Mech. Astron.* **53**, 127408 (2023).
- [20] V. V. Kabanov, J. Demsar, B. Podobnik, and D. Mihailovic, *Phys. Rev. B* **59**, 1497 (1999).
- [21] J. Demsar, J. L. Sarrao, and A. J. Taylor, *J. Phys.: Condens. Matter* **18**, R281 (2006).
- [22] Y. Z. Zhao, Q. Y. Wu, C. Zhang, B. Chen, W. Xia, J. J. Song, Y. H. Yuan, H. Liu, F. Y. Wu, X. Q. Ye, H. Y. Zhang, H. Huang, H. Y. Liu, Y. X. Duan, Y. F. Guo, J. He, and J. Q. Meng, *Phys. Rev. B* **108**, 075115 (2023).
- [23] K. S. Burch, E. E. M. Chia, D. Talbayev, B. C. Sales, D. Mandrus, A. J. Taylor, and R. D. Averitt, *Phys. Rev. Lett.* **100**, 026409 (2008).
- [24] Y. P. Liu, Y. J. Zhang, J. J. Dong, H. Lee, Z. X. Wei, W. L. Zhang, C. Y. Chen, H. Q. Yuan, Y. F. Yang, and J. Qi, *Phys. Rev. Lett.* **124**, 057404 (2020).
- [25] J. Qi, T. Durakiewicz, S. A. Trugman, J. X. Zhu, P. S. Riseborough, R. Baumbach, E. D. Bauer, K. Gofryk, J. Q. Meng, J. J. Joyce, A. J. Taylor, and R. P. Prasankumar, *Phys. Rev. Lett.* **111**, 057402 (2013).
- [26] A. Rothwarf and B. N. Taylor, *Phys. Rev. Lett.* **19**, 27 (1967).
- [27] V. Iyer, Y. P. Chen, and X. F. Xu, *Phys. Rev. Lett.* **121**, 026807 (2018).
- [28] P. Sharma, A. Bhardwaj, R. Sharma, V. P. S. Awana, T. N. Narayanan, K. V. Raman, and M. Kumar, *J. Phys. Chem. C* **126**, 11138(2022).
- [29] Y. Li, H. Deng, C. Wang, S. Li, L. Liu, C. Zhu, K. Jia, Y. Sun, X. Du, X. Yu, T. Guan, R. Wu, S. Zhang, Y. Shi, and H. Mao, *Acta Phys. Sin.* **70**, 186801 (2021).
- [30] See Supplemental Material at **** for additional experimental results and a supporting data analysis, which includes Refs.[12, 31–36].
- [31] D. Lim, R. D. Averitt, J. Demsar, A. J. Taylor, N. Hur, and S. W. Cheong, *Appl. Phys. Lett.* **83**, 4800 (2003).
- [32] M. Takahara, H. Jinn, S. Wakabayashi, T. Moriyasu, and T. Kohmoto, *Phys. Rev. B* **86**, 094301 (2012).
- [33] D. Wang, A. Cross, G. Guarino, S. Wu, R. Sobolewski, and A. Mycielski, *Appl. Phys. Lett.* **90**, 211905 (2007).
- [34] F. H. Yu, H. M. Mu, W. Z. Zhuo, Z. Y. Wang, Z. F. Wang, J. J. Ying, and X. H. Chen, *Phys. Rev. B* **102**, 180404(R) (2020).
- [35] B. Xu, P. Marsik, S. Sarkar, F. Lyzwa, Y. Zhang, B. Shen, and C. Bernhard, *Phys. Rev. B* **103**, 245101 (2021).
- [36] Q. Wu, T. Hu, D. Wu, R. Li, L. Yue, S. Zhang, S. Xu, Q. Liu, T. Dong, and N. Wang, *Phys. Rev. B* **107**, 174411 (2023).
- [37] H. Li, S. Y. Gao, S. F. Duan, Y. F. Xu, K. J. Zhu, S. J. Tian, J. C. Gao, W. H. Fan, Z. C. Rao, J. R. Huang, J. J. Li, D. Y. Yan, Z. T. Liu, W. L. Liu, Y. B. Huang, Y. L. Li, Y. Liu, G. B. Zhang, P. Zhang, T. Kondo, S. Shin, H. C. Lei, Y. G. Shi, W. T. Zhang, H. M. Weng, T. Qian, and H. Ding, *Phys. Rev. X* **9**, 041039 (2019).
- [38] P. E. Majchrzak, Y. Liu, K. Volckaert, D. Biswas, C. Sahoo, D. Puntel, W. Bronsch, M. Tuniz, F. Cilento, X. Pan, Q. Liu, Y. P. Chen, S. Ulstrup, *Nano Letters* **23**, 414 (2023).
- [39] R. Lu, H. Y. Sun, S. Kumar, Y. Wang, M. Q. Gu, M. Zeng, Y. J. Hao, J. Y. Li, J. F. Shao, X. M. Ma, Z. Y. Hao, K. Zhang, W. Mansuer, J. W. Mei, Y. Zhao, C. Liu, K. Deng, W. Huang, B. Shen, K. Shimada, E. F. Schwier, C. Liu, Q. H. Liu, C. Y. Chen, *Phys. Rev. X* **11**, 011039 (2021).
- [40] Y. S. Wang, B. Chen, Z. T. Liu, X. Guo, S. You, Z. Wang, H. Xie, T. Niu, J. Q. Meng, and H. Huang, *Phys. Rev. B* **108**, 045118 (2023).
- [41] R. V. Yusupov, T. Mertelj, J. H. Chu, I. R. Fisher, and D. Mihailovic, *Phys. Rev. Lett.* **101**, 246402 (2008).
- [42] M. F. Collins, *Magnetic critical scattering* (Oxford University Press, 1989).
- [43] D. Afanasiev, J. R. Hortensius, M. Matthiesen, S. Mañas-Valero, M. Siškins, M. Lee, E. Lesne, H. S. J. van der Zant, P. G. Steeneken, B. A. Ivanov, E. Coronado, and A. D. Caviglia, *Sci. Adv.* **7**, f3096 (2021).
- [44] A. M. Kalashnikova, A. V. Kimel, R. V. Pisarev, V. N. Gridnev, A. Kirilyuk, and T. Rasing, *Phys. Rev. Lett.* **99**, 167205 (2007).
- [45] J. Nishitani, T. Nagashima, and M. Hangyo, *Appl. Phys. Lett.* **103**, 081907 (2013).
- [46] T. Parpiiev, A. Hillion, V. Vlasov, V. Gusev, K. Dumesnil, T. Hauet, S. Andrieu, A. Anane, T. Pezeril, *Phys. Rev. B* **104**, 224426 (2021).
- [47] Y. Shin, M. Vomir, D. Kim, P. C. Van, J. Jeong, J. Kim, *Communications Physics* **5**, 56 (2022).
- [48] K. Shinozaki, Y. Goto, K. Hoshi, R. Kiyama, N. Nakamura, A. Miura, C. Moriyoshi, Y. Kuroiwa, H. Usui, and Y. Mizuguchi, *ACS Appl. Energy Mater.* **4**, 5155 (2021).
- [49] D. S. Wu, S. H. Na, Y. J. Li, X. B. Zhou, W. Wu, Y. T. Song, P. Zheng, Z. Li, and J. L. Luo, *Phys. Chem. Chem. Phys.* **26**, 8695 (2024).
- [50] V. A. Stoica, D. Puggioni, J. Zhang, R. Singla, G. L. Dakovski, G. Coslovich, M. H. Seaberg, M. Kareev, S. Middey, P. Kissin, R. D. Averitt, J. Chakhalian, H. Wen, J. M. Rondinelli, and J. W. Freeland, *Phys. Rev. B* **106**, 165104 (2022).